

Cabinet and Shelter Vibration Isolation: Numerical and Experimental Investigation

G. Di Massa, S. Pagano, S. Strano

Abstract—Passive isolation systems are often adopted to reduce vibrating energy acting on a sensitive equipment due to external sources as machinery, road/rail traffic, earthquakes, etc.

The paper describes a theoretical and experimental investigation conducted on a steel light structure, simulating a cabinet or a shelter containing sensitive equipment. It is isolated from the ground seismic acceleration by means of four isolators each consisting of a ball transfer unit (BTU) and a wire rope spring (WRS). This kind of isolator has hysteretic non-linear behaviour with damping caused by the dry friction due to the wires relative motion; the non-linear stiffness and damping is function of the wire rope configuration and on its diameter and length.

Some experimental tests have been performed to characterize the isolator and to obtain an analytical description of its dynamic behaviour; then the steel light structure, supported by four WRS-BTU isolators, has been tested on a shake-table to evaluate the isolation efficiency. The experimental results have been compared with the theoretical ones obtained with a numerical model in which the isolator hysteretic behaviour has been modelled with the Bouc-Wen theory. The validated model has been then used to simulate the cabinet dynamic response due to recorded seismic ground motion.

Index Terms—Seismic Isolators, Bouc-Wen, Nonlinear Dynamics, Wire Rope, Vibration Isolation.

I. INTRODUCTION

Tough and durable cabinets and shelters are used for housing electro-mechanical and electronic high-tech items (as devices for telecommunications, control systems, power equipment, etc.) having a vital role of work in many industries and often placed in very harsh operating environments.

They assure protection against weathering, spread of fire, noise, etc. Some shelters have to support antennas and satellite dishes for signal emission and/or reception. Sometimes, both internal and external devices must be protected against vibrations and they must operate even during a seismic event.

G. Di Massa is with the *Dipartimento di Ingegneria Industriale, Università degli Studi di Napoli Federico II*, 80125 ITALY, (e-mail: giandomenico.dimassa@unina.it).

S. Pagano is with the *Dipartimento di Ingegneria Industriale, Università degli Studi di Napoli Federico II*, 80125 ITALY, (e-mail: pagano@unina.it).

S. Strano is with the *Dipartimento di Ingegneria Industriale, Università degli Studi di Napoli Federico II*, 80125 ITALY, (corresponding author, phone:+390817683277; e-mail:salvatore.strano@unina.it).

Seismic passive isolation requires the use of devices with high vertical stiffness, in order to avoid large compliances due to the weight of the structure, and low horizontal stiffness to shift the natural period away from the period range having the most of earthquake energy.

All base isolation systems have certain common features such as re-centring capability and energy absorbing capacity; they can be divided into three main types: elastomeric, rolling and sliding devices.

The most common isolators are the elastomeric steel-reinforced ones that are made up of elastomeric layers alternated with steel sheets, whose number and size are chosen to obtain a high vertical stiffness and a low horizontal stiffness.

Rolling isolators are instead constituted by two parallel rigid plates with interposed rolling bodies. As an example, Fig. 1 shows a rolling device with three steel balls rolling on a plate; the balls sustain a disk on which is connected the structure to be isolated. The isolator is equipped with three pre-stressed helical steel springs able to re-centre the disk and other three helical springs to re-centre the balls cage-spacer; the horizontal stiffness depends on the direction and amplitude of the disk displacement as shown in the polar diagram reported in Fig. 2a. As three (or more than three) isolators constitute the isolation system, it is possible to properly orient them to obtain a quite rounded stiffness polar diagram (Fig. 2b).



Fig. 1. Rolling seismic isolator with helical springs (DII, Naples, Italy).

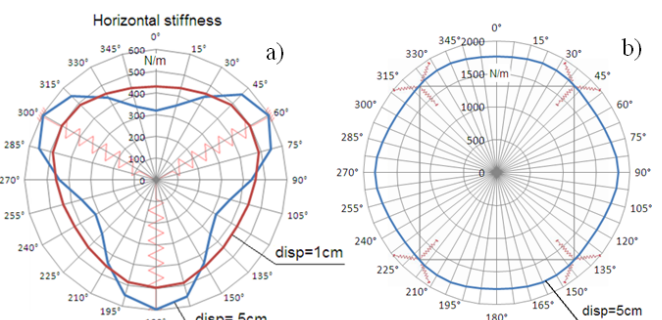


Fig. 2. Horizontal stiffness polar diagram: a) single isolator; b) four isolators.

Several types of rolling supports are now available. For example, two linear recirculating ball guides orthogonally arranged (Fig. 3), to allow movement along any horizontal directions, constitute the THK support. Fig. 4 reports the rolling device proposed by M. Ismail et al. [1], made up of a stiff rolling body placed between the superstructure and substructure, respectively.

The sliding isolators mainly consist of a teflon disk, supporting the structure, that slides on a stainless steel plate. Sliding and rolling supports can be realized with sloped or spherical surfaces so that a relative horizontal displacement, between superstructure and substructure, generates a gravitational restoring force and a dissipative force due to friction [2]. Both devices are generally characterized by a friction coefficient equal to about 3%.

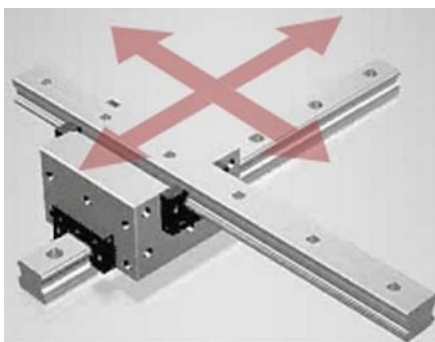


Fig. 3. THK rolling device (from: www.thk.com).

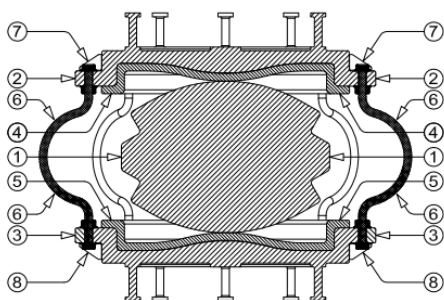


Fig. 4. Ismail et al. rolling isolator.

Fig. 5a shows the scheme of sloped rolling-type isolation devices. The roller can also be constituted by cylinders placed between two V-shaped sloping surfaces [3]. In [4] an approximate expression is derived for predicting the peak acceleration response of a structure isolated by the rolling-type isolators, as there is a lower-bound PGA for triggering a sloped rolling mechanism.

Fig. 5b represents the scheme of the single friction pendulum system (FPS) that is a sliding device with spherical surfaces. The structure natural frequency is selected simply by choosing the radius of curvature of the concave surface.

The present paper describes the dynamic behaviour of a rolling isolator that can be used to isolate light structures or sensitive equipments housed in cabinets or shelters. The isolator [5] is very simple and cheap; it consists (Fig. 6) of two plates between which it is placed a ball transfer unit (BTU) that has the task of supporting the cabinet weight allowing horizontal relative displacements with low friction. The restoring force is provided by some ropes connecting the two plates, making up a wire rope spring (WRS). This kind of spring, with respect to most common rubber ones,

has a longer service life since they are not very sensitive to temperature changes and resists aggressive environments caused by the presence of ozone, oil, grease and salt spray; they dissipate energy due to friction between the wires. It is characterized by a hysteretic non-linear behaviour depending on the configuration, the diameter and the length of the selected wire rope.

The described isolator can be considered as an extension of the mono-directional device introduced by Demetriades et al. [6], constituted by a combination of a wire rope spring and a locked castored wheel.

This paper reports a theoretical and experimental investigation on the seismic isolation of a light mass structure, as a cabinet, adopting WRS-BTU isolators.

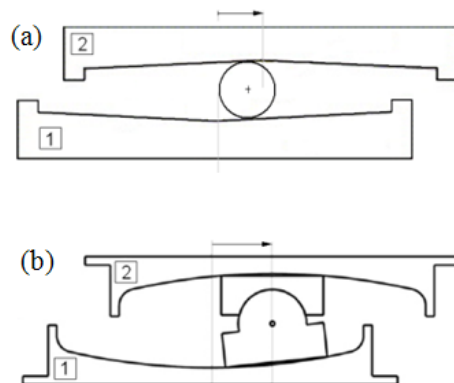


Fig. 5. a) Rolling device with sloped surface; b) Sliding device with spherical surfaces (friction pendulum system, FPS).

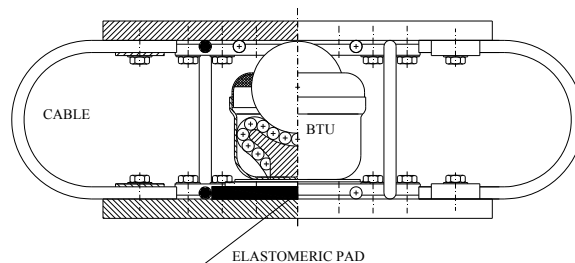


Fig. 6. WRS-BTU isolator.

The experimental characterization of the isolator has been performed adopting the BPI testing machine [7], available at the DII laboratory, which allows to impose a horizontal periodic shear force to the device with a constant vertical compression (Fig. 7). The mobile platform of the machine (Fig. 8) has been then adopted as a vibrating shake-table on which the isolated cabinet has been tested.

In [8] the results of some experimental investigations are

reported; in particular, starting from the hysteretic cycles, deduced by shear tests, the equivalent stiffness and damping have been derived. Then, the results of an experimental modal analysis, carried out on the isolated cabinet has been presented to highlight the isolation performances.

Some linear and nonlinear analytical models have been tested to describe the isolator restoring force [9]. In the following, the analytical results obtained with a nonlinear model, based on a modified Bouc-Wen model, are reported and compared with the experimental ones. The validated model has also been used to simulate the cabinet dynamic response due to seismic excitations, some results are reported in section IV.

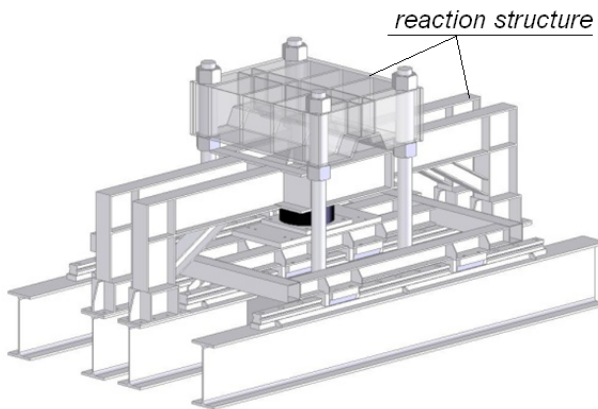


Fig. 7. BPI testing machine.

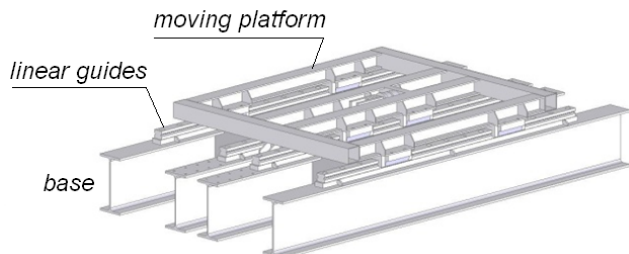


Fig. 8. BPI adopted as shake-table.

II. WRS-BTU ISOLATOR CHARACTERIZATION

The isolator is constituted by 8 cables; each one has a length of 90 mm and a diameter of 5 mm. Some characterization tests have been performed using the BPI testing machine; the isolator upper plate has been horizontally locked and has been loaded with a vertical constant force; the lower plate has been fixed on the platform, excited with a harmonic motion.

The controller of the hydraulic actuator, employed to move the platform, must ensure the tracking of the target displacement in presence of the unknown restoring force of the isolation devices. For this reason, a control based on a mixed approach has been adopted; it is constituted by a model inversion based control, coupled with a feedback contribution [7]. To this aim, a non-linear model for the hydraulic actuation system has been derived and adopted for the feedforward synthesis through the inverse dynamics resolution. As a consequence, feedback control has the function to compensate for the tracking error due to model

uncertainties and the unknown isolator reaction force. This control criterion allows to design a control action that results minimally invasive on the stability characteristics and allows to obtain good tracking results without the increasing of the feedback control gain.

The test rig is instrumented to detect the following measurements:

- table position y by means of magnetostrictive position sensor (FS = 0.4 m - estimated uncertainty = $\pm 1.2E-4$ m);
- actuation force by means of strain gauge load cell (FS = 250000 N - estimated uncertainty = ± 500 N);
- vertical load pressing on the specimen under test by means of strain gauge load cell (FS = 1E6 N - estimated uncertainty = ± 230 N);
- platform and cabinet accelerations by means of two piezoelectric accelerometers.

Since the BPI has been designed to characterize more rigid isolators, the sensitivity of the load cell and the friction forces of the platform linear guides do not allow to make accurate investigation for the isolator described in the present paper. For this reason, a suitable device has been realized (Figs. 9 and 10). It is made up of a slide horizontally connected to the BPI platform by means of a load cell and vertically supported by four BTUs; two couples of rolling bearing laterally guide the slide.



Fig. 9. Device for the characterization of isolator stiffness.

The load cell is characterized by FS = 1335 N; estimated uncertainty is equal to ± 0.13 N.

When the platform moves, the following forces act on the slide (Fig. 10b):

- isolator restoring force, F ;
- inertia force of the slide mass and of the isolator bodies connected to the slide (lower plate and isolator BTU), $m_s \ddot{x}$;
- friction forces of four BTUs supporting the slide: $4F_f$;
- horizontal constraint force (measured by load cell), F_{LC} .

Therefore, the expression for the restoring force F is:

$$F = F_{LC} - m_s \ddot{x} - 4F_f \quad (1)$$

The inertia force, $m_s \ddot{x}$, is obtained from the measurement of the slide horizontal acceleration and the knowledge of the

mass m_s .

The friction force, exerted by the four supporting BTUs, is: $F_f = f_s N$, being N the vertical load and f_s the friction coefficient.

Fig. 11 shows the results of some tests carried out by imposing sinusoidal deformation law with an equal amplitude A (0.03m) and three different values of frequency f (0.1, 0.5; 1 Hz). In each case, the cycle has been obtained with and without the contact between the BTU and the bearing surface to put in evidence the BTU rolling resistance due to a vertical load of 1220N, smaller than the maximum allowed, equal to 1400N.

The detected cycles show that:

- without contact between BTU and bearing surface, the cycle area increases with the forcing frequency; the wire rope spring is therefore characterized even by a viscous damping;
- the contact between BTU and bearing surface leads to a further increment of the cycle area;
- the device has a hardening behaviour more marked at low frequencies and for greater deformation of the cables.

Fig. 12 shows other tests conducted without BTU contact, for three different frequency values and with the same amplitude of 0.02m; the behaviour is similar to the one shown in Fig. 11.

The experimental cycles have been used to define analytically the isolator restoring force that mainly depends on the instantaneous ropes deformation, on the deformation velocity and on the history of the ropes deformation [9].

The isolator reaction F has been modelled as the sum of the following two components:

$$F(t) = F_c(t) + F_r(t) \tag{2}$$

where, F_c represents the wire ropes action and $F_r(t) = f_r N \text{sgn}(\dot{x}(t))$ is the BTU rolling friction force.

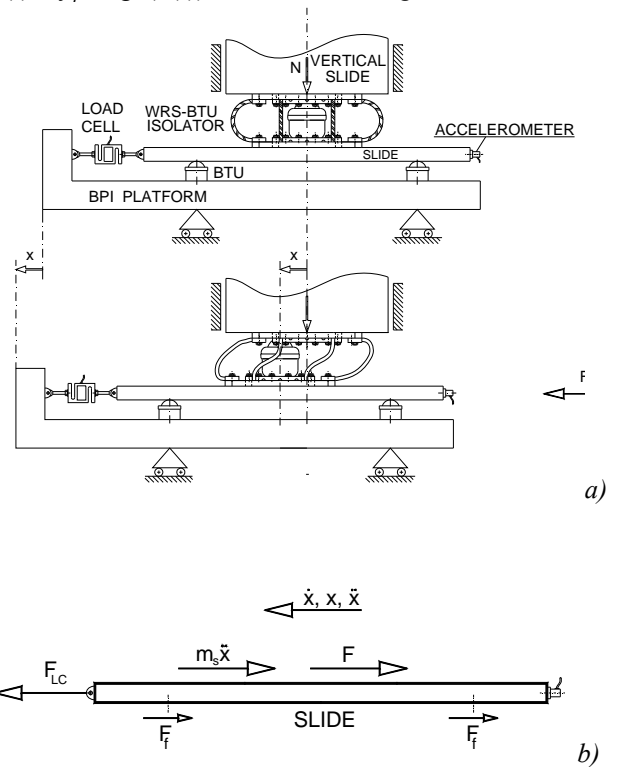


Fig. 10. Device for the characterization of isolator stiffness: a) scheme; b) forces acting on the slide.

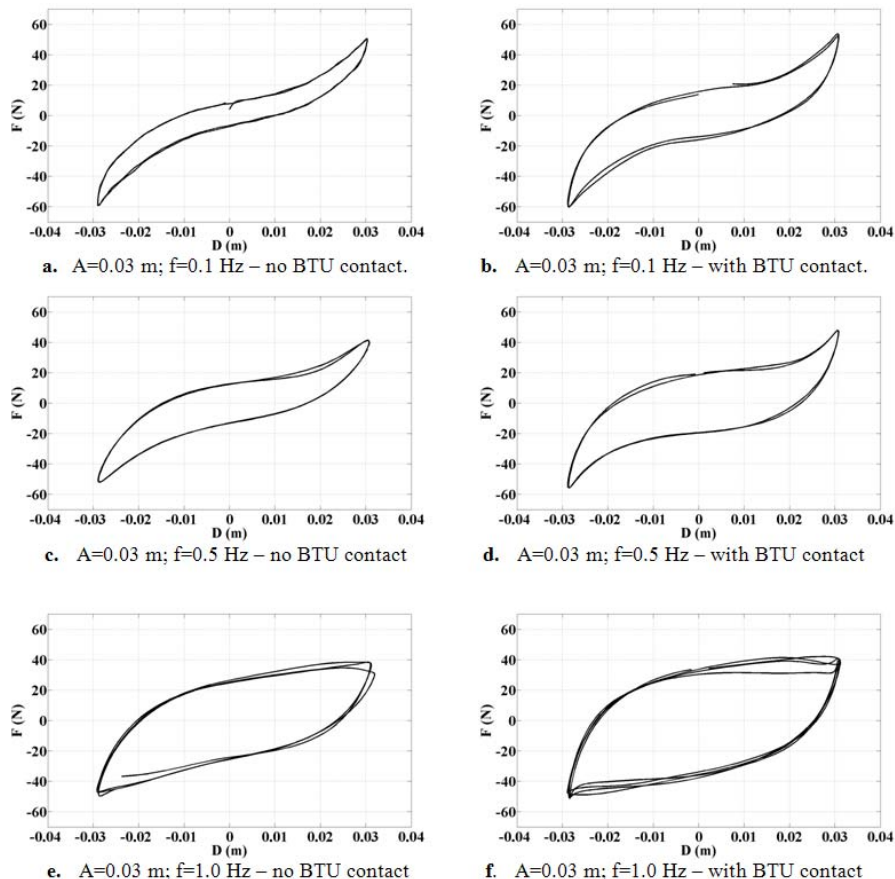


Fig. 11. Force-displacement cycles for different frequencies, with amplitude of 30mm.

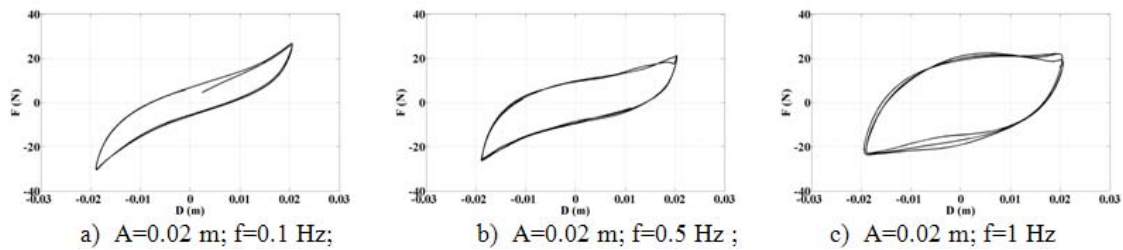


Fig. 12. Force-displacement cycles for different frequencies in no BTU contact condition.

In the following, the analytical expressions of the above components are reported in order to obtain a model that can be used to describe the isolator dynamic behaviour.

The F_c component has been modelled as the sum of four independent terms:

$$F_c(t) = F_{el}(t) + F_h(t) + F_{nl}(t) + F_v(t) \quad (3)$$

where: $F_e(t) = k_e x(t)$, is the elastic component, proportional to the displacement $x(t)$; F_h is the hysteretic component; $F_{nl}(t) = k_{nl} x(t)^3$, is a non-linear component proportional to the cube of the displacement, and $F_v(t) = \sigma_v \dot{x}(t)$, is the viscous damping component.

The hysteretic component has been derived from a simplified version of the Bouc-Wen model presented in [10]:

$$F_h(t) = k_w w(t) \quad (4)$$

$$\dot{w}(t) = \rho \dot{x}(t) [1 - \text{sgn}(\dot{x}(t))w(t)]$$

where ρ and k_w are positive parameters that change the shape of the cycle. By appropriately choosing these two last parameters, it is possible to accommodate the response of the model to the real hysteresis loops; the use of system identification techniques is a practical way to perform this task [11].

The identification procedure has been conducted adopting the least mean squared method between experimental and theoretical data. In Table I the identified parameter are reported.

TABLE I
WRS-BTU FORCE MODEL PARAMETERS

Model parameter	k_e	k_{nl}	σ_v	f_r	ρ	k_w
Value	1000	900000	90	0.005	800	6.25
Unit	N/m	N/m ³	Ns/m	-	1/m	N

The comparisons between the numerical and experimental results are shown in Figs. 13 and 14; the figures highlight that the numerical model results are satisfactory. The main differences are due to the asymmetries of the experimental cycles caused by the unavoidable asymmetries of the isolator. The model results are in good accordance with the experimental ones even in the case of BTU contact as shown in Fig. 14b.

Therefore, the isolator model can be used to evaluate the isolation effectiveness of structures isolated with these devices, for different structures inertial characteristics and/or

for different kinds of excitations.

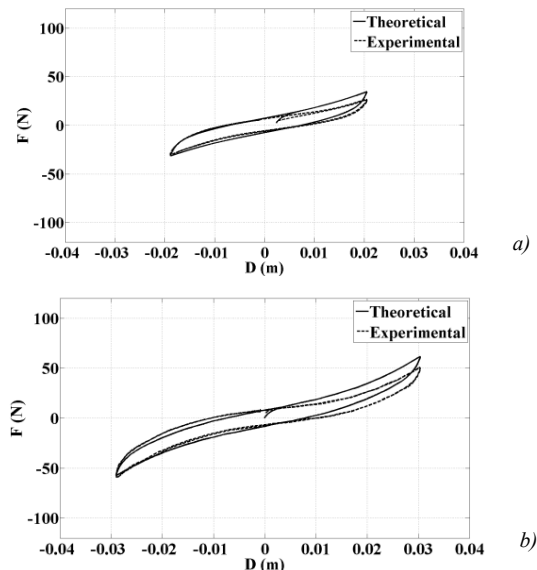


Fig. 13. Comparison between theoretical and experimental cycle for $f=0.1$ Hz and without BTU contact. Amplitude: a) 0.02m; b) 0.03m..

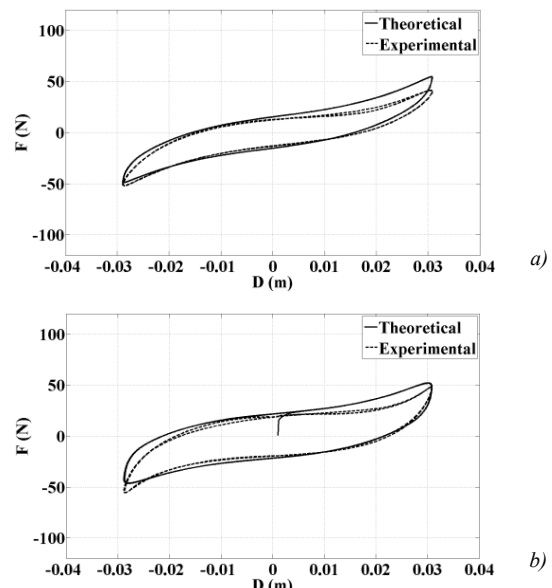


Fig. 14. Comparison between theoretical and experimental cycle for $f=0.5$ Hz, $A=0.03$ m. a) without BTU contact; b) with BTU contact.

In the following sections the model is adopted to predict the dynamic behaviour of a light steel structure excited by a harmonic ground motion; the theoretical results are compared with the experimental ones. Afterwards, the same model is adopted to predict the dynamic response of structures subjected to seismic excitation.

III. CABINET FREQUENCY ANALYSIS

WRS-BTU isolators have been adopted to isolate a laboratory cabinet (Figs. 15 and 16) constituted of a rigid steel frame (0.60 x 0.70 x 1.20 m) on which may be fixed additional masses to modify the inertial properties. The tests have been conducted with the cabinet overall mass of 165 kg placed on the moving platform of the BPI, driven by a position-controlled hydraulic actuator [12]. The controller of the platform hydraulic actuator, even when the BPI testing machine works as a shaking-table, assures a good tracking of the target displacement. Also in this BPI utilization, the forces acting on the platform are unknown. In this case, the cabinet transmits forces to the platform, depending on its dynamics, which, in turn, are related to the platform movement and to the isolator characteristics.



Fig. 15. Cabinet on the shake-table.



Fig. 16. Cabinet isolators and additional masses.

The additional masses have been arranged in the lower part of the cabinet to avoid the cabinet overturning.

In order to characterize the isolated cabinet in the frequency domain, the input motion to the platform of the shaking table has been chosen of harmonic type. The tests have been conducted for two different values of the amplitude and forcing frequency in the 0.5–5.0 Hz range. By means of two accelerometers, platform and cabinet acceleration have been detected and the two time histories have been compared.

As the platform movement is not perfectly harmonic, for each test, a frequency analysis of the two time histories (platform and cabinet accelerations) has been performed. The amplitudes of the components, synchronous with that imposed to the platform, have been compared.

The ratio (a_c/a_g) of the acceleration synchronous components, versus the forcing frequency (Fig. 17), shows a peak in the neighbourhood of 1 Hz; this frequency may be considered as a resonant frequency. The system is then isolated for forcing frequencies greater than about 1.5 Hz. This threshold value depends on the motion amplitude as shown by the two curves obtained for two different platform motion amplitude (5 and 10 mm).

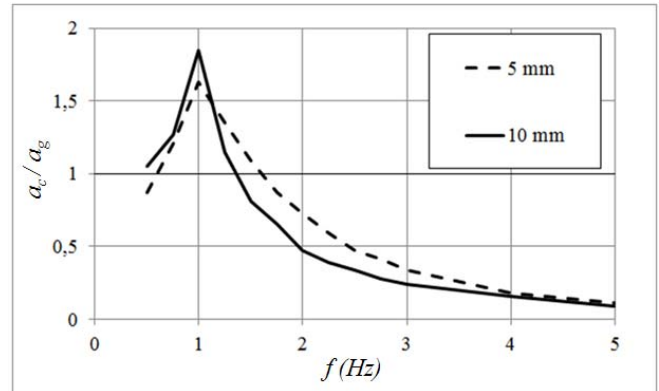


Fig. 17. Acceleration ratio vs. forcing frequency.

It must be noted that for linear systems the acceleration ratio, if defined as a_c/a_g (i.e. output/input), is equivalent to the correspondent displacement ratio d_c/d_g , also known as “displacement transmissibility”:

$$T = a_c / a_g = (d_c \omega^2 / d_g \omega^2) = d_c / d_g \tag{5}$$

being ω the exciting circular frequency. For this reason, the experimental acceleration ratio has a qualitative shape (Fig. 17) that resembles the linear displacement transmissibility of vibrating linear systems, characterized by a peak amplitude in correspondence of the resonant frequency and very low values for high frequencies.

The acceleration signals have been compared with those ones coming from the numerical integration of the motion equations in which the isolator behaviour is modelled as indicated in the previous paragraph. The motion equations are based on the assumption that the cabinet centre of the masses coincides with isolators stiffness centre; under this hypothesis, the cabinet can be considered as a single degree of freedom system.

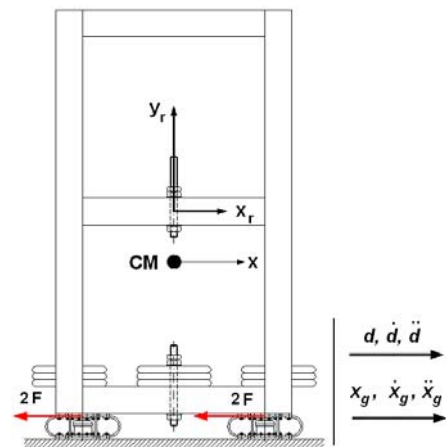


Fig. 18. Cabinet sketch.

The cabinet motion equation is:

$$m_c \ddot{x} + 4F = 0 \tag{6}$$

being (Fig. 18):

- $x(t)$, cabinet displacement;
- F , the restoring force exerted by each isolator;
- m_c , the mass of the cabinet.

Indicating with $x_g(t)$ the ground (platform) displacement, the relative displacement between cabinet and ground is:

$$d(t) = x(t) - x_g(t) \tag{7}$$

The simulations regard the dynamic behaviour of the cabinet forced to vibrate by a harmonic ground acceleration:

$$\ddot{x}_g(t) = a_g \sin(\omega t) \tag{8}$$

where a_g is the platform horizontal acceleration amplitude. The corresponding platform displacement has the following form:

$$x_g(t) = -\frac{a_g}{\omega^2} \sin(\omega t) \tag{9}$$

Therefore the cabinet equation, in term of relative motion, is:

$$m_c \ddot{d} + 4F = -m_c \ddot{x}_g \tag{10}$$

The numerical simulations have been performed imposing to the platform a harmonic displacement law characterized by amplitude and forcing frequency in accordance with those ones assigned for the experimental investigation.

In Fig. 19 a comparison between the numerical and experimental results is reported for three different values of the forcing frequency and equal platform amplitude displacement (0.01m).

For each forcing frequency, the comparisons between theoretical and experimental cabinet acceleration show a good agreement; the differences can be even attributed to a slight yaw rotation of the cabinet detected by the accelerometer and to the unavoidable dissymmetry of the isolators.

The numerical code can be considered validated and so it has been adopted to describe the dynamic system behaviour.

As an example in the same Fig. 19 the platform absolute displacements (d_p) versus the cabinet ones (d_c) and the trend of the restoring force (F) versus the relative displacement (d), are reported.

In accordance with Fig. 17, the first diagrams type (d_p vs. d_c), show that for a given platform displacement amplitude (0.01m), the cabinet motion is amplified at about 1 Hz while it is isolated for higher frequencies (3 Hz).

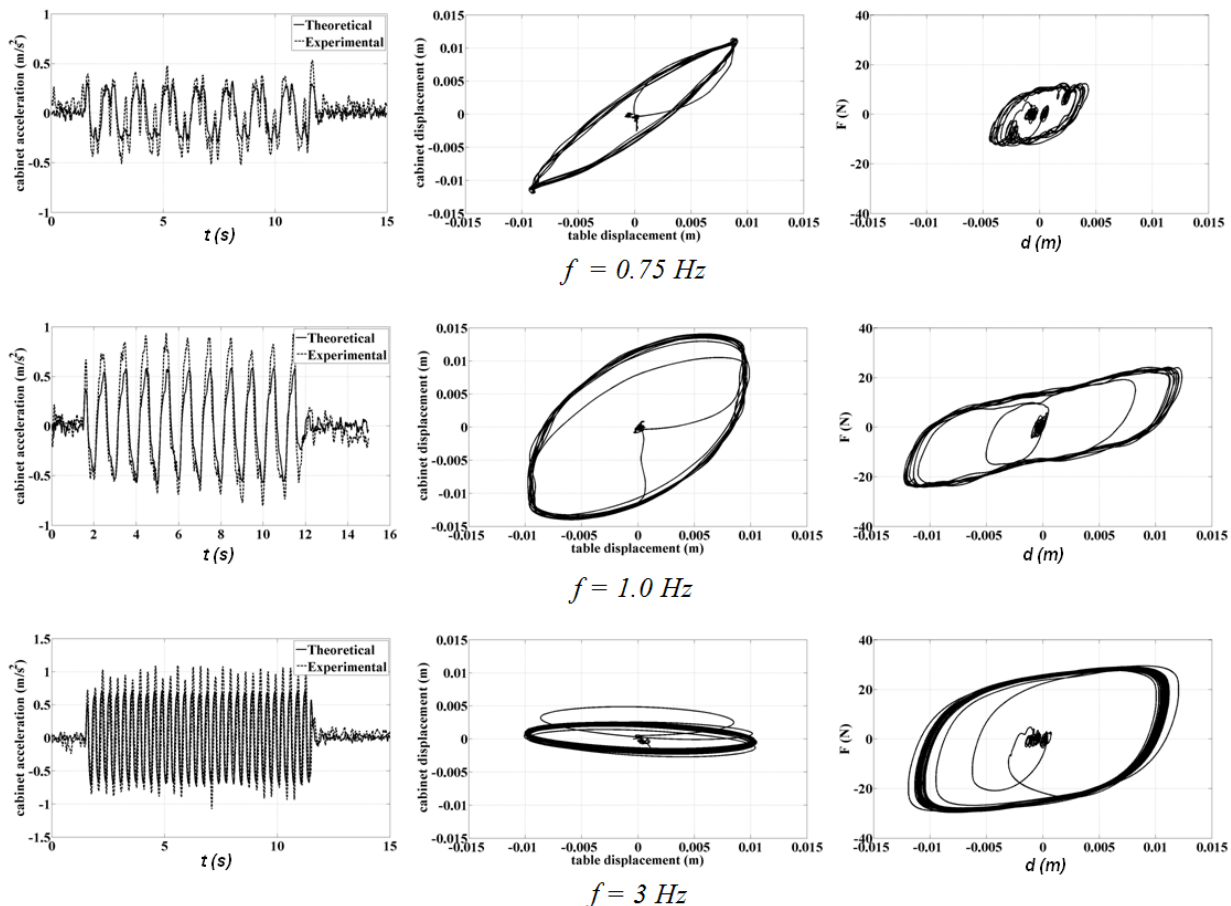


Fig. 19. Comparison between experimental and theoretical acceleration; platform displacements (d_p) versus the cabinet displacements (d_c); restoring force (F) versus the relative displacement (d).

The F - d diagrams are characterized by cycles whose areas represent the energy dissipation due to the presence of hysteresis, viscous damping and friction. It can be noted that the areas increase with the forcing frequency showing an evident viscous contribute. Moreover, due to the presence of friction, the equilibrium position is not univocal as highlighted in the F - d diagrams, where the final equilibrium position does not coincide with the initial one.

For the forcing frequency equal to 3 Hz the relative motion appears rather large, while the absolute cabinet displacement is significantly lower than the platform one. This condition of isolation is so characterized by large restoring force, large energy dissipation and small absolute cabinet motion amplitude.

The displacement transmissibility (d_c/d_g) has been deduced adopting the simulation code. For an assigned ground harmonic displacement amplitude (d_g) and circular frequency (ω), the cabinet time history has been evaluated. The ratio between the amplitude of their fundamental harmonic components amplitude has been plotted versus the forcing frequency f (Fig. 20). The curve has a qualitative trend similar to the experimental ones reported in Fig. 17.

The acceleration transmissibility is defined, similarly to linear systems, as:

$$T_a = d_c \omega^2 / d_g \quad (8)$$

(In linear vibrating systems, this quantity is divided for the squared natural circular frequency and therefore it is a dimensionless ratio).

The correspondent diagram shows that the cabinet acceleration rapidly grows with forcing frequency, until the resonant frequency (1 Hz); then, the acceleration continues to grow although with a lower slope (Fig. 21).

In seismic applications, both displacement and acceleration transmissibility have particular importance; it is necessary to contain the maximum displacement value to avoid excessive stresses in the connections of the structure with the neighboring plants (pipes, wires, etc.) and to not exceed the maximum isolator deformation; besides, it is necessary to limit structure acceleration to contain inertia forces.

The damping of the isolation system contains the maximum cabinet acceleration reached in resonance condition.

A trade-off between displacement and acceleration amplitudes can be obtained in the frequency range 1-2 Hz.

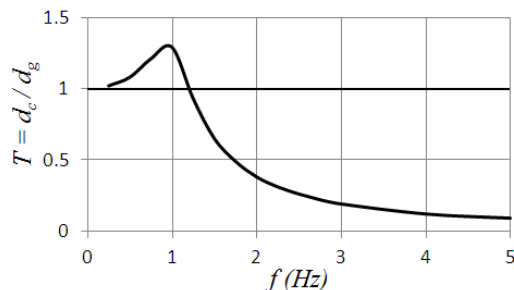


Fig. 20. Displacement transmissibility ($d_g = 10$ mm)

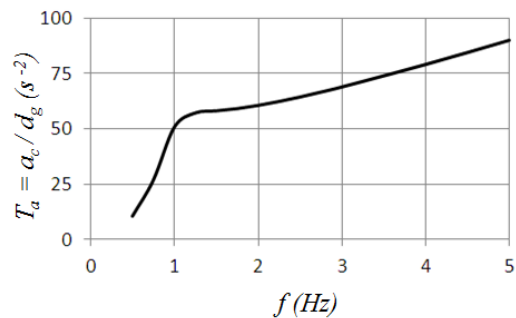


Fig. 21. Acceleration/displacement ratio ($d_g = 10$ mm)

IV. CABINET SEISMIC RESPONSE

The good agreement between theoretical and experimental results, highlighted in the previous section, in case of harmonic ground acceleration, allows the proposed model to be used even to simulate different base excitations and in particular seismic ones.

The reported results have been obtained considering as ground excitation the horizontal time history acceleration of the *Irpinia* earthquake (Italy, 1980) [13]. Simulations have been repeated by scaling the accelerogram in order to take into account the hardening characteristic of the insulator. Figs. 22, 23 and 24 report the simulation results for the following scale factor (SF): 0.50; 1.0; 1.5.

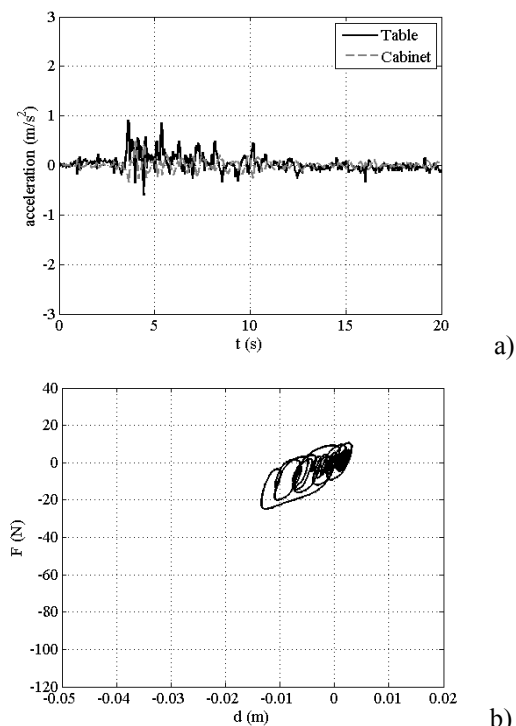


Fig. 22. Comparison between ground and cabinet acceleration with SF=0.5; a) accelerograms (acceleration ratio = 1.9); b) restoring force vs. relative displacements.

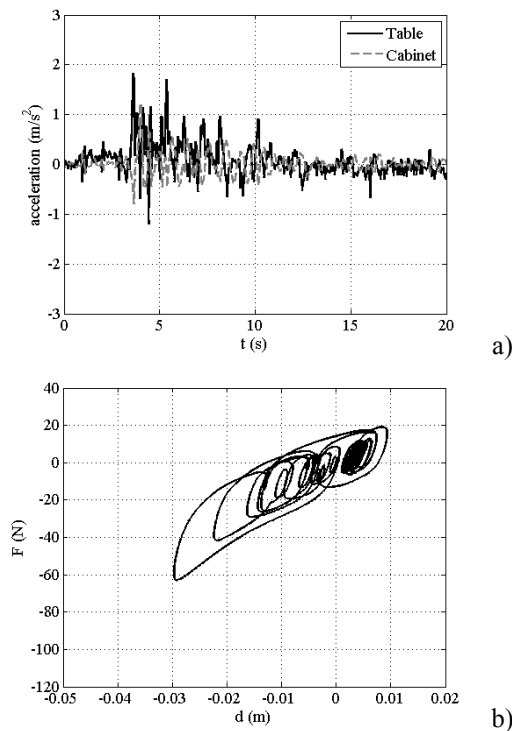


Fig. 23. Comparison between ground and cabinet acceleration with SF=1; a) accelerograms (acceleration ratio = 1.5); b) restoring force vs. relative displacements.

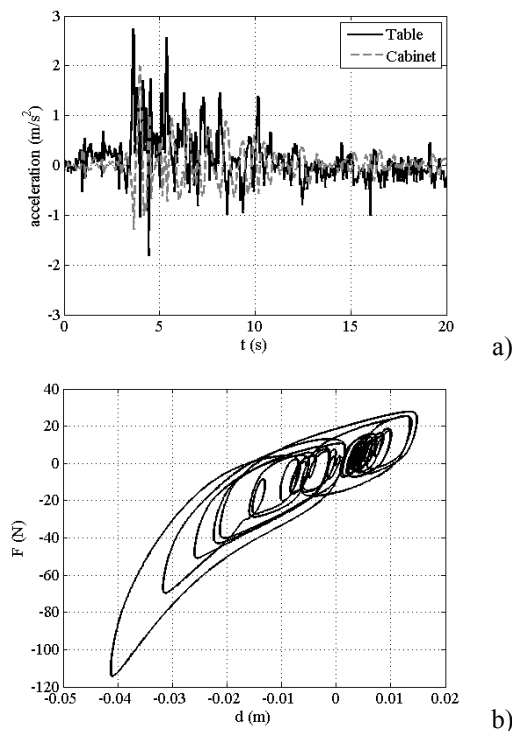


Fig. 24. Comparison between ground and cabinet acceleration with SF=1.5; a) accelerograms (acceleration ratio = 1.4); b) restoring force vs. relative displacements.

Examining diagram it can be observed that:

- a_c/a_g (intended in this case as the ratio between ground and cabinet peak acceleration) decrease with SF; it varies from 1.9 to 1.4 for SF=0.5 and SF=1.5, respectively;
- passive seismic protection decreases with ground acceleration;
- cabinet peak displacements is lower than the maximum allowed displacement (about 50mm);

- restoring force vs. relative displacement has the typical shape of the hardening isolators characterized by an evident increase of the force in the final part of the stroke.

V.CONCLUSION

In this paper, a numerical method useful to simulate and predict the dynamic behaviour of cabinets or shelters, equipped with WRS-BTU devices, is presented.

A survey to assess the efficiency of the isolation system has been conducted. The proposed isolator is cheap and easy to realize by coupling a BTU with WRS springs; both the components are easily obtainable from industrial production and are already characterized by the manufacturers. In the design stage, a suitable horizontal stiffness can be easily obtained to set the desired system natural frequency. Moreover, the two components must not necessarily be integrated in a single unit.

The proposed numerical model has been validated and then has been used to simulate the cabinet dynamic response due to a seismic ground motion. The effectiveness of the isolation device has been evaluated comparing the ground acceleration diagram with the corresponding cabinet one.

REFERENCES

- [1] M. Ismail, J. Rodellar, F. Ikhouane, "An innovative isolation bearing for motion-sensitive equipment," *Journal of Sound and Vibration*, vol. 326, no. 3-5, pp.503-521, Oct. 2009.
- [2] A. Mokha, M. Constantinou, A. Reinhorn, V. Zayas, "Experimental Study of Friction Pendulum Isolation System," *J. Struct. Eng.*, vol. 117, no. 4, pp. 1201-1217, 1991.
- [3] S.J. Wang, C.H. Yu & J.Y. Hsiao, "Development of Sloped Rolling-Type Isolation Devices for Seismic Protection of Important Equipment and Facilities," *15th World Conference in Earthquake Engineering*, Lisboa, 2012.
- [4] M.H. Tsaia, S.Y. Wub, K.C. Change, G.C. Leed, "Shaking table tests of a scaled bridge model with rolling-type seismic isolation bearings," *Engineering Structures*, vol. 29, no. 5, pp. 694-702, May 2007.
- [5] G. Di Massa, S. Pagano, E. Rocca, S. Strano, "Sensitive equipments on WRS-BTU isolators," *Meccanica*, vol. 48, no. 7, pp. 1777-1790, 2013.
- [6] G.F. Demetriades, M.C. Constantinou, A.M. Reinhorn, "Study for wire rope systems for seismic protection of equipment in buildings," *Engineering Structures*, vol. 15, no. 5, pp. 321-334, September 1993.
- [7] S. Pagano, M. Russo, S. Strano, M. Terzo, "Seismic isolator test rig control using high-fidelity non-linear dynamic system modeling," *Meccanica*, vol. 49, no. 1, pp. 169-179, 2014.
- [8] R. Brancati, G. Di Massa, S. Pagano, E. Rocca, S. Strano, "Experimental investigation of the performances of a WRS-BTU seismic isolator", *World Congress on Engineering*, London, U.K., 3-5 July, 2013.
- [9] G. Di Massa, S. Pagano, S. Strano, F. Timpone, "A comparison between linear and nonlinear modelling of a wire rope seismic isolator," *International Review on Modelling and Simulations*, vol. 6, no. 4, pp. 1307-1313, Aug. 2013.
- [10] M. Ismail, F. Ikhouane, J. Rodellar, "The Hysteresis Bouc-Wen Model, a Survey," *Arch. Comput. Methods Eng.*, vol. 16, no.2, pp. 161-188, 2009.
- [11] I.I. Lazaro, A. Alvarez, J. Anzurez, "The Identification Problem Applied to Periodic Systems Using Hartley Series," *Engineering Letters*, vol. 21, no.1, pp. 36 - 43, Feb. 2013.
- [12] S. Strano, M. Terzo, "A first order model based control of a hydraulic seismic isolator test rig," *Engineering Letters*, vol. 21, no. 2, pp. 52 - 60, 2013.
- [13] N. Ambraseys, P. Smit, R. Sigbjornsson, P. Suhadolc, B. Margaris, "Internet-Site for European Strong-Motion Data," *European Commission, Research-Directorate General, Environment and Climate Program 2002*. http://www.isesd.hi.is/ESD_Local/frameset.htm [24 July 2013].